This article has been accepted for publication in IEEE Transactions on Vehicular Technology. This is the author's version which has not been fully edited and content may change prior to final publication. Citation information: DOI 10.1109/TVT.2022.3141949

Stochastic Fading Channel Models with Multiple Dominant Specular Components

Juan M. Romero-Jerez, F. Javier Lopez-Martinez, Juan P. Peña-Martín and Ali Abdi

***Abstract*— We introduce a comprehensive statistical characterization of the multipath wireless channel built as a superposition of scattered waves with random phases. We consider an arbitrary number N of specular (dominant) components plus an undetermined number of other weak diffusely propagating waves. Our approach covers the cases in which the specular components have constant amplitudes, as well as when these components experience random fluctuations. We show that this class of fading models can be expressed in terms of a continuous mixture of an underlying Rician (or Rician shadowed) fading model, averaged over the phase distributions of the specular waves. The proposed model parameters can be adjusted to tailor the statistical distribution of the received radio signal power to a wide variety of wireless scenarios, some of which are not covered by other state-of-the-art stochastic wireless channel models. In this regard, we verify that the proposed models accurately fit experimental measurements for which their multi-modality cannot be properly captured by other current stochastic models. It is shown that the fluctuations of the specular components have a detrimental impact on performance, and it is formally demonstrated that the lower error rate is obtained when the signal power is concentrated on a single specular component, regardless of whether it fluctuates or not.**

***Index Terms*—Wireless channel modeling, statistical characterization, multipath propagation, small-scale fading.**

I. Introduction

With the advent of every new generation of mobile communications, the need for providing high data rates with a low latency and a high reliability pushes the very limits of communication systems and techniques as we know them. The huge variety of use cases considered for 5G [1], which include device-to-device, machine-to machine and vehicular communications, among many others, entails that such performances are attained in rather dissimilar situations. Because the nature of the wireless channel strongly depends on the operation environment, an accurate characterization of these new wireless propagation scenarios is required.

J. M. Romero-Jerez and F. Javier Lopez-Martinez are with Communications and Signal Processing Lab, Instituto Universitario de Investigación en Telecomunicación (TELMA), Universidad de Málaga, CEI Andalucía TECH, ETSI Telecomunicación, Bulevar Louis Pasteur 35, 29010 Málaga (Spain). Contact e-mail: romero@dte.uma.es.

Juan P. Peña-Martín is with Departmento de Tecnología Electrónica and with Instituto de Telecomunicación (TELMA), Universidad de Málaga, CEI Andalucía TECH , Málaga 29071, Spain.

Ali Abdi is with Dept. Electrical and Computer Engineering, New Jersey Institute of Technology, Newark, NJ 07102, USA.

The work of J.M. Romero-Jerez, F. Javier Lopez-Martinez and J.P. Peña-Martin was funded by the Spanish Government, Junta de Andalucia and the European Fund for Regional Development FEDER (projects TEC2017-87913-R and P18-RT-3175).

A. Related work

There has been a great deal of effort in the development of advanced channel models in the context of 5G, aiming to incorporate the geometry of transmitter, receiver and the environment into the channel model [2, 3]. This approach, which combines geometric aspects together with stochastic channel modeling, is useful to recreate realistic propagation conditions in a synthetic form. However, due to the large amount of parameters involved in their definition, their use for predicting the behavior of wireless communication systems operating in these environments is far from practical.

In the most general set-up, the received radio signal is formed by the superposition of a set of individual waves, each of which may have a different amplitude and phase [4]. With this formulation, and based on the assumption of a sufficiently large number of received waves, the central limit theorem (CLT) applies and the classical Rician and Rayleigh fading models emerge for the cases when, respectively, there is or there is not a dominant wave. In case that such condition does not hold, the distribution of the received signal largely differs from a Gaussian-like distribution. The statistical characterization of the wireless channel where the CLT does not fully apply becomes relevant again today in the context of 5G: for instance, in mmWave communications the diffuse scattering is reduced and only a finite number of multipath components arrives at the receiver [5]. Similarly, the consideration of ray-based fading models has an important impact in the tail behavior for ultra-reliable and low-latency communications [6] or physical layer security [7]. Recently, the use of intelligent reflecting surfaces to modify at will the amplitudes and phases [8, 9] of the scattered waves to improve the system performance also justifies the need for a deeper knowledge of the statistics for the equivalent channel.

The statistical characterization of the distribution of the received radio signal is related to one of the key problems in communication theory: the distribution of the sum of N random phase vectors, which is also equivalent to the random walk problem in general statistics. While this problem has been addressed [10–13] by some of the most reputed communication theorists, its inherent complexity makes it very challenging to characterize its chief statistics. In the context of stochastic channel modeling, it is worth mentioning the pioneering works in [14, 15], which set the foundations for later advances in the field [16–18]. From a practical perspective, manageable (although in integral form) expressions for the probability density function (PDF) and the cumulative distribution function (CDF) are only available for $N = 2$,

giving raise to the popular two wave with diffuse power (TWDP) fading model [16]. However, as a larger number of specular components is considered, i.e., $N > 2$, the numerical evaluation of the PDF and CDF becomes rather hard [11]. Expansions based on Laguerre polynomial series [19], multivariate hypergeometric functions or using the Hankel transform (which requires an improper integration of a highly oscillatory function) are no exception [20].

B. Contributions

In this paper, we present a new approach to the characterization of wireless channels built as a superposition of N specular waves plus a diffuse component[1]. The key contributions of this paper can be listed as follows:

- By conveniently expressing the received signal power in terms of an underlying conditional Rician-like distribution, its PDF, CDF and moment generating function (MGF) are obtained for any arbitrary N. The resulting expressions require for the evaluation of definite integrals (between 0 and 2π) of a smooth integrand.
- Our approach has additional benefits from a performance analysis viewpoint, and allows for easily incorporating a random fluctuation on the amplitude of the specular waves, thus generalizing the class of fading models defined in [18] for arbitrary N.
- It is shown that dramatic modifications in the distribution of the radio signal power can be obtained from the proposed models when $N = 3$ with respect to that of well known models for $N = 1$ and $N = 2$. This allows the proposed models to be applied to a wider range of wireless scenarios.

C. Organization of the paper

The remainder of this paper is structured as follows: the physical underpinnings of a ray-based fading model with constant-amplitude specular components is introduced in Section II, and its statistical characterization is then carried out in Section III in terms of its PDF, CDF and MGF. Then, in Section IV, the proposed model is generalized to consider random fluctuations of the specular components. A formal proof that the lowest MGF is obtained when there is a single specular component is presented in Section V, which has important implications in the achievable error rates. Performance of wireless communication systems operating under these fading models and empirical verification with field measurements are exemplified in Section VI. Finally, the key conclusions are summarized in Section VII.

[1]We note that these channels differ from the multiple-order scattering fading (MOSF) models proposed in [21, 22]. The MOSF models are built as a combination of a single dominant specular component and a finite number of increasing-order scattering terms associated to the diffuse component of the fading model. This provides a wider flexibility in circumstances where the central limit theorem does not apply for the diffuse component –e.g. in the case of keyhole propagation – at the expense of a prohibitive mathematical complexity. In this sense, the family of N-wave fading models here analyzed and the family of MOSF models are different by construction, as they are targeted to model different propagation conditions

II. System Model

The signal in a wireless multipath fading channel can be modeled as the superposition of a set of N dominant waves, referred to as specular components, to which other M diffusely propagating waves are added [16]. The received signal can be expressed as

$$R\exp(j\phi) = \sum_{i=1}^{N} a_i \exp(j\theta_i) + \underbrace{\sum_{i=1}^{M} A_i \exp(j\phi_i)}_{A_d = X + jY}, \quad (1)$$

where $a_i \exp(j\theta_i)$ represents the *i-th* specular component, which is assumed to have a constant amplitude a_i and a uniformly distributed random phase θ_i, such that $\theta_i \sim \mathcal{U}[0, 2\pi)$, where the random phase variables of each specular component are assumed to be statistically independent. Under the assumption that the diffuse received signal component is due to the combined reception of numerous weak, independently-phased scattered waves, then the CLT applies *for this component* and hence we can approximate the last term in (1), i.e., A_d, as a complex Gaussian random variable, such that $X, Y \sim \mathcal{N}(0, \sigma^2)$. Let Ω_0 denote the average power of the diffuse component. Thus, we can write $E\{|A_d|^2\} = \Omega_0 = 2\sigma^2$, where $E[\cdot]$ denotes the expectation operator.

We note that the model described in (1) includes the Rayleigh fading model as a special case for $N = 0$, i.e., no specular component is present. For $N = 1$, i.e., a single dominant specular component, we have the Rician fading model. The case in which there are two dominant specular components ($N = 2$) is usually referred to as the TWDP fading model, originally proposed by Durgin, Rappaport and de Wolf [16]. Our aim will be pursuing the statistical characterization of the model in (1) for arbitrary N. For consistence with the usual nomenclature in the context of fading channel modeling, this will be referred to as the N-Wave with Diffuse Power (NWDP) fading model.

III. Statistical characterization of NWDP fading

A. Calculation of the PDF and CDF

Let us define the superposition of the specular components as

$$B_N \exp(j\Psi_N) \triangleq \sum_{i=1}^{N} a_i \exp(j\theta_i), \quad (2)$$

where B_N and Ψ_N denote the resulting amplitude and phase, respectively, of the additive combination of the dominant specular components, so that (1) becomes

$$R\exp(j\phi) = B_N \exp(j\Psi_N) + A_d. \quad (3)$$

Note that according to [23] the distribution of R is independent of the distribution of Ψ_N, thanks to the circular symmetry of A_d. Conditioned on B_N, we have that R follows a Rician distribution, and its PDF will be given by

$$f_{R|B_N}(r|B_N) = \frac{2r}{\Omega_0} \exp\left(-\frac{r^2 + B_N^2}{\Omega_0}\right) I_0\left(\frac{2B_N r}{\Omega_0}\right), \quad (4)$$

where $I_0(\cdot)$ is the zeroth-order modified Bessel function of the first kind.

This article has been accepted for publication in IEEE Transactions on Vehicular Technology. This is the author's version which has not been fully edited and content may change prior to final publication. Citation information: DOI 10.1109/TVT.2022.3141949

Let us define

$$P_N \triangleq B_N^2 = \left(\sum_{i=1}^{N} a_i \cos(\theta_i)\right)^2 + \left(\sum_{i=1}^{N} a_i \sin(\theta_i)\right)^2, \quad (5)$$

which can be rewritten, with the help of the multinomial theorem, as

$$P_N = \Omega_N + 2\sum_{\Delta_N} a_i a_k \cos(\theta_i - \theta_k) \quad (6)$$

with $\Delta_N = \{(i,k) : i < k,\ i = 1...N-1,\ k = 2...N\}$, and where Ω_N denotes the total average power of the specular components, verifying

$$\Omega_N \triangleq E[P_N] = \sum_{i=1}^{N} a_i^2. \quad (7)$$

Let us define the power envelope of the received signal $U \triangleq R^2$. The PDF of U will be obtained by averaging over P_N as

$$f_U(u) = E_{P_N}\left[\frac{1}{\Omega_0}\exp\left(-\frac{u+P_N}{\Omega_0}\right) I_0\left(\frac{2}{\Omega_0}\sqrt{P_N u}\right)\right], \quad (8)$$

and the CDF will be given by

$$F_U(u) = 1 - E_{P_N}\left[Q\left(\sqrt{\frac{2P_N}{\Omega_0}}, \sqrt{\frac{2u}{\Omega_0}}\right)\right], \quad (9)$$

where $Q(\cdot,\cdot)$ is the first-order Marcum Q-function. Similarly, and leveraging the asymptotic approximation for the Rician CDF in [24], we can also obtain an asymptotic expression for (9), as the total average power $\Omega = \Omega_N + \Omega_0 \to \infty$

$$\begin{aligned} F_U(u) \approx & \frac{u}{\Omega_0} \cdot E_{P_N}\left[\exp\left(-\frac{P_N}{\Omega_0}\right)\right] \\ = & \frac{u(K_N+1)}{\Omega} \exp(-K_N) E_{f(\theta)}\left[\exp\left(-\frac{f(\theta)}{\Omega_0}\right)\right], \end{aligned} \quad (10)$$

with $f(\theta) = 2\sum_{\Delta_N} a_i a_k \cos(\theta_i - \theta_k)$ as in (6), and where we used $K_N = \Omega_N/\Omega_0$ as a generalization of the Rician K factor. From (10) we see that the diversity order (i.e. the exponent of u/Ω) is one $\forall N$, and the power offset (i.e., the scale factor of u/Ω) depends on the power of the dominant components in a very simple form. These are new results in the literature to the best of our knowledge.

Without any loss of generality, let us assume that $\theta_1 = 0$. From (5) and (6), averaging over P_N is equivalent to averaging over $\theta_2, ..., \theta_N$, i.e., $N-1$ nested integrals in the interval $[0, 2\pi)$ need to be computed. This kind of computation is rather common in communication theory [25] and actually does not pose any numerical challenge to our results because the integrand is a continuous bounded function and the integration interval is finite. In addition, the case $N > 4$ will rarely need to be considered, as the proposed model will rapidly converge to either Rayleigh or Rician fading (depending on whether or not the underlying complex Gaussian random variable has zero mean) by virtue of the central limit theorem [16, 20].

The results in this section indicate that the distribution of the NWDP fading model can be viewed as an underlying Rician distribution with a continuously varying power of the specular component, which is given by the random variable P_N. This indicates that any performance metric for the NWDP fading model can be calculated from existing results for Rician fading by averaging over P_N (or, equivalently, over $\theta_2, ..., \theta_N$). We will now see that the calculation of the MGF becomes simpler than the PDF and CDF expressions, since additional manipulations will allow to eliminate one nested finite-integral. This implies, for instance, that the case with $N = 2$ dominant specular components can be obtained in closed-form, whereas $N-2$ finite-range integrations need to be performed for arbitrary $N > 2$, i.e. a finite-range single integral will need to be computed for $N = 3$ and an easy-to-compute double integral will be required for $N = 4$.

B. Calculation of the MGF

The MGF of the envelope power U, conditioned on the instantaneous power of the specular components, P_N, can be calculated as

$$\begin{aligned} & M_N(s|P_N) = \\ & \frac{1}{\Omega_0}\int_0^\infty \exp\left(su - \frac{u+P_N}{\Omega_0}\right) I_0\left(\frac{2}{\Omega_0}\sqrt{P_N u}\right) du \\ & \quad = \frac{1}{1-\Omega_0 s}\exp\left(\frac{P_N s}{1-\Omega_0 s}\right). \end{aligned} \quad (11)$$

It has been shown in [26] that P_N can be computed recursively as

$$P_N = P_{N-1} + a_N^2 + 2a_N\sqrt{P_{N-1}}\cos(\theta_N - \Psi_{N-1}), \quad (12)$$

where $P_0 = 0$. Therefore, we can express the MGF of U conditioned on P_{N-1}, θ_N and Ψ_{N-1} as

$$\begin{aligned} & M_N(s|P_{N-1}, \theta_N, \Psi_{N-1}) = \frac{1}{1-\Omega_0 s} \\ & \times \exp\left(\frac{\left(P_{N-1} + a_N^2 + 2a_N\sqrt{P_{N-1}}\cos(\theta_N - \Psi_{N-1})\right)s}{1-\Omega_0 s}\right). \end{aligned} \quad (13)$$

Considering that $I_0(x) = 1/(2\pi)\int_0^{2\pi}\exp(x\cos(\beta-\xi))d\xi$, the dependency on θ_N and Ψ_{N-1} can be eliminated in (13) by computing

$$M_N(s|P_{N-1}) = \frac{1}{2\pi}\int_0^{2\pi} M_N(s|P_{N-1}, \theta_N, \Psi_{N-1}) d\theta_N, \quad (14)$$

yielding

$$\begin{aligned} M_N(s|P_{N-1}) = & \frac{1}{1-\Omega_0 s}\exp\left(\frac{\left(P_{N-1}+a_N^2\right)s}{1-\Omega_0 s}\right) \\ & \times I_0\left(\frac{2a_N\sqrt{P_{N-1}}s}{1-\Omega_0 s}\right). \end{aligned} \quad (15)$$

The unconditional MGF will thus be given by:

$$\begin{aligned} & M_N(s) = \frac{1}{1-\Omega_0 s} \\ & \times E_{P_{N-1}}\left[\exp\left(\frac{\left(P_{N-1}+a_N^2\right)s}{1-\Omega_0 s}\right) I_0\left(\frac{2a_N\sqrt{P_{N-1}}s}{1-\Omega_0 s}\right)\right]. \end{aligned} \quad (16)$$

The recursive expression of P_N given in (12) was helpful to obtain (16); however, the practical use of (12) in order to perform the expectation operation in (16) can be cumbersome. A more practical expression of P_N for this purpose is given in (6). We note that the MGF of the pure N-Ray model (i.e. without diffuse component) is obtained as a by-product by setting $\Omega_0 = 0$, i.e.:

$$M_N(s)|_{\Omega_0=0} = e^{a_N^2 s} E_{P_{N-1}}\left[e^{sP_{N-1}} I_0\left(2a_N\sqrt{P_{N-1}}s\right)\right], \tag{17}$$

which is another new result.

For $N = 1$ no averaging is needed and, as expected, (16) collapses to the well known MGF of the squared Rician distribution, i.e.

$$M_1(s) = \frac{1}{1-\Omega_0 s}\exp\left(\frac{a_1^2 s}{1-\Omega_0 s}\right). \tag{18}$$

When $N = 2$, since $P_1 = a_1^2$ is a constant, there is no need to average, and (16) results in

$$M_2(s) = \frac{1}{1-\Omega_0 s}\exp\left(\frac{\left(a_1^2+a_2^2\right)s}{1-\Omega_0 s}\right) I_0\left(\frac{2a_1a_2 s}{1-\Omega_0 s}\right), \tag{19}$$

which is the MGF of a squared TWDP distribution, derived in [17] for the first time. By comparing (16) and (19) it can be concluded that the distribution of the NWDP fading model can also be viewed as the distribution of the TWDP fading model with continuous varying power of one of the two specular components, which is given by the random variable P_{N-1}. Therefore, any performance metric for the NWDP fading model can be calculated from existing results for TWDP fading by averaging over P_{N-1} or, equivalently, over $\theta_2, ..., \theta_{N-1}$, thus involving $N-2$ integrations. Although there are less closed-form known expressions of performance metrics for the TWDP fading as compared to Rician fading, some relevant closed-form results were presented in [27] for the TWDP fading model.

When $N = 3$, the MGF can be efficiently calculated by performing a finite-range integral in $[0, 2\pi)$, as in this case, from (16), we can write

$$M_3(s) = \frac{1}{1-\Omega_0 s} \times E_{\theta_2}\left[\exp\left(\frac{\left(P_2+a_3^2\right)s}{1-\Omega_0 s}\right) I_0\left(\frac{2a_3\sqrt{P_2}s}{1-\Omega_0 s}\right)\right], \tag{20}$$

where $P_2 = a_1^2 + a_2^2 + 2a_1a_2\cos\theta_2$.

Similarly, for $N = 4$, the MGF can be computed by performing a double finite-range integral in $[0, 2\pi)$, as in this case we have

$$M_4(s) = \frac{1}{1-\Omega_0 s} \times E_{\theta_2,\theta_3}\left[\exp\left(\frac{\left(P_3+a_4^2\right)s}{1-\Omega_0 s}\right) I_0\left(\frac{2a_4\sqrt{P_3}s}{1-\Omega_0 s}\right)\right], \tag{21}$$

where $P_3 = a_1^2 + a_2^2 + a_3^2 + 2a_1a_2\cos\theta_2 + 2a_1a_3\cos\theta_3 + 2a_2a_3\cos(\theta_2-\theta_3)$.

IV. A GENERALIZATION OF NWDP FADING

The specular components in the general model in (1) have constant amplitudes. We note that in some instances, variations in the amplitudes of the dominant specular components occur. This phenomenon has been considered in some scenarios and validated with field measurements: these are the cases of the Rician shadowed fading model [28] or the Fluctuating Two-Ray (FTR) fading model [18], where the amplitudes of the specular components are assumed to be modulated by a normalized gamma random variable[2]. Generalizing this approach, we can write:

$$R\exp(j\phi) = \sum_{i=1}^{N}\sqrt{\zeta}a_i\exp\left(j\theta_i\right) + X + jY, \tag{22}$$

where ζ is a unit-mean Gamma distributed random variable with PDF

$$f_\zeta(u) = \frac{m^m u^{m-1}}{\Gamma(m)}e^{-mu}, \tag{23}$$

where m is the shape parameter in charge of modelling the severity of the fluctuation of ζ. For instance, low values of m are associated with a more severe fluctuation, whereas large values of m indicate a milder fluctuation. Note that we are considering the same fluctuation for the specular components, which is a natural situation in different wireless scenarios in which the scatterers are in the vicinity of the transmitter and/or the receiver, as discussed in [18].

The wireless channel model given in (22)-(23) for the particular case when $N = 1$ corresponds to the Rician shadowed fading model [28] and when $N = 2$ corresponds to the FTR fading model [18]. For the sake of shorthand notation, and in coherence with the standing nomenclature in wireless channel modeling, this general ray-based model with fluctuating dominant specular components will be referred to as the Fluctuating N-Ray (FNR) fading model and, to the authors' knowledge, its statistical characterization has not been presented for $N > 2$ in a tractable form [20].

A. Calculation of the PDF and CDF

Let us define P_N as in (5) and (6). Conditioning on P_N, and following the same rationale as in the previous Section, the FNR fading model reduces to a conditional Rician shadowed fading model. Thus, using [28, eq. (6)] the distribution of the received power envelope of the FNR model will be given by

$$f_U(u) = E_{P_N}\left[\left(\frac{\Omega_0 m}{\Omega_0 m + P_N}\right)^m \frac{1}{\Omega_0}\exp\left(-\frac{u}{\Omega_0}\right) \times {}_1F_1\left(m;1;\frac{P_N u}{\Omega_0\left(\Omega_0 m + P_N\right)}\right)\right], \tag{24}$$

[2]Note that this is equivalent to consider that the specular components experience a Nakagami fading, which is a well established wireless fading model validated by field measurements [25].

where ${}_1F_1(\cdot)$ is the confluent hypergeometric function of the first kind. With the help of [29, eq. (8)], the CDF can be written

$$F_U(u) = \frac{u}{\Omega_0} E_{P_N}\left[\left(\frac{\Omega_0 m}{\Omega_0 m + P_N}\right)^m \times \Phi_2\left(1-m; m; 2; -\frac{u}{\Omega_0}; -\frac{mu}{\Omega_0 m + P_N}\right)\right], \tag{25}$$

where Φ_2 is the bivariate confluent hypergeometric function defined in [30, p. 34, (8)]. Note that when the fading parameter m is a positive integer, then the PDF and CDF of the Rician shadowed model are given in terms of a finite sum of powers and exponentials [29]. In this situation, the consideration of a random fluctuation in the specular components brings additional benefits from a practical perspective, as the numerical integration of these functions is always simpler than its deterministic counterpart.

An asymptotic expression for the CDF similar to that in (10) can be obtained using [31] as

$$F_U(u) \approx \frac{u}{\Omega_0} \cdot E_{P_N}\left[\left(\frac{m}{\frac{P_N}{\Omega_0} + m}\right)^m\right]. \tag{26}$$

Again, the diversity order of the FNR fading model is one for arbitrary N.

B. Calculation of the MGF

Conditioning on P_N, the MGF can be written with the help of [28, eq. (7)][3] as

$$M_N\left(s|P_N\right) = \frac{m^m\left(1-\Omega_0 s\right)^{m-1}}{\left(m - \left(m\Omega_0 + P_N\right)s\right)^m}. \tag{27}$$

Let us define

$$\beta\left(P_{N-1}\right) \triangleq m\Omega_0 + P_{N-1} + a_N^2. \tag{28}$$

Introducing (12) into (27), we can write

$$M_N(s|P_{N-1}, \theta_N, \Psi_{N-1}) = \frac{m^m\left(1-\Omega_0 s\right)^{m-1}}{\left(m - \left(\beta\left(P_{N-1}\right) + 2a_N\sqrt{P_{N-1}}\cos\left(\theta_N - \Psi_{N-1}\right)\right)s\right)^m}. \tag{29}$$

Let us now assume that parameter m takes integer values for the sake of simplicity. Averaging with respect to the random variable θ_N and noticing that the function given in (29) is periodic with period 2π with respect to this variable, with the help of [32, eq. 3.661.4], we can obtain

$$M_N(s) = E_{P_{N-1}}\left[\frac{m^m\left(1-\Omega_0 s\right)^{m-1}}{\left(\sqrt{\left[m - \beta\left(P_{N-1}\right)s\right]^2 - 4a_N^2 P_{N-1} s^2}\right)^m} \times \mathcal{P}_{m-1}\left(\frac{m - \beta\left(P_{N-1}\right)s}{\sqrt{\left[m - \beta\left(P_{N-1}\right)s\right]^2 - 4a_N^2 P_{N-1} s^2}}\right)\right], \tag{30}$$

[3]Which can be written in a more compact form with respect to the expression given in the reference.

where $\mathcal{P}_n(\cdot)$ is the Legendre polynomial of degree[4] n, which can be written as [33, p. 775 (22.3.8)]

$$\mathcal{P}_n\left(z\right) = \frac{1}{2^n}\sum_{q=0}^{\lfloor n/2\rfloor}(-1)^q C_q^n z^{n-2q}, \tag{31}$$

where $\lfloor\cdot\rfloor$ is the floor function and C_q^n is a coefficient given by

$$C_q^n = \left(\begin{array}{c} n \\ q \end{array}\right)\left(\begin{array}{c} 2n-2q \\ n \end{array}\right) = \frac{(2n-2q)!}{q!\,(n-q)!\,(n-2q)!}. \tag{32}$$

When $N = 1$, we can write

$$M_1(s) = \frac{m^m\left(1-\Omega_0 s\right)^{m-1}}{\left(m - \left(m\Omega_0 + a_1^2\right)s\right)^m}, \tag{33}$$

while for $N = 2$ we have

$$M_2(s) = \frac{m^m\left(1-\Omega_0 s\right)^{m-1}}{\left(\sqrt{\left[m - \left(m\Omega_0 + a_1^2 + a_2^2\right)s\right]^2 - 4a_1^2 a_2^2 s^2}\right)^m} \times \mathcal{P}_{m-1}\left(\frac{m - \left(m\Omega_0 + a_2^2 + a_2^2\right)s}{\sqrt{\left[m - \left(m\Omega_0 + a_1^2 + a_2^2\right)s\right]^2 - 4a_1^2 a_2^2 s^2}}\right), \tag{34}$$

which, after some manipulation, can be shown to be equivalent to the MGF of the FTR fading model given in [18, eq. (8)].

The obtained results indicate that the FNR fading model is equivalent to the Rician shadowed fading model when, for any realization of ζ, the power of the specular component is given by the random variable P_N. Alternatively, by comparing (30) and (34), the FNR fading model can also be viewed as the as the FTR fading model with continuous varying power of one of the two specular components (again, for any realization of ζ), which is given by the random variable P_{N-1}. Therefore, any performance metric for the FNR fading model can be calculated from existing results for the Rician shadowed model and averaging over P_N (which involves $N-1$ finite-range integrations) or from results for the FTR fading by averaging over P_{N-1} (involving $N-2$ integrations in this case).

When $N = 3$, the MGF can be calculated by performing a finite-range integral in $[0, 2\pi)$, as in this case, from (30), we have

$$M_3(s) = E_{\theta_2}\left[\frac{m^m\left(1-\Omega_0 s\right)^{m-1}}{\left(\sqrt{\left[m - \beta\left(P_2\right)s\right]^2 - 4a_3^2 P_2 s^2}\right)^m} \times \mathcal{P}_{m-1}\left(\frac{m - \beta\left(P_2\right)s}{\sqrt{\left[m - \beta\left(P_2\right)s\right]^2 - 4a_3^2 P_2 s^2}}\right)\right], \tag{35}$$

where $\beta\left(P_2\right) = m\Omega_0 + P_2 + a_3^2$, with $P_2 = a_1^2 + a_2^2 + 2a_1 a_2\cos\theta_2$.

[4]Relaxing the assumption of $m \in \mathbb{Z}^+$ implies that (30) is expressed in terms of the Legendre function $\mathcal{P}_{m-1}(z)$ [18], which is related to the Gauss Hypergeometric function as $\mathcal{P}_\mu(z) = {}_2F_1(-\mu, \mu+1; 1; \frac{1-z}{2})$.

For $N = 4$ a double integration in $[0, 2\pi)$ is required, as in this case we can write

$$M_4(s) = E_{\theta_2,\theta_3}\left[\frac{m^m\left(1-\Omega_0 s\right)^{m-1}}{\left(\sqrt{\left[m-\beta\left(P_3\right)s\right]^2 - 4a_4^2P_3s^2}\right)^m} \times \mathcal{P}_{m-1}\left(\frac{m-\beta\left(P_3\right)s}{\sqrt{\left[m-\beta\left(P_3\right)s\right]^2 - 4a_4^2P_3s^2}}\right)\right], \tag{36}$$

where $\beta\left(P_3\right) = m\Omega_0 + P_3 + a_4^2$, with $P_3 = a_1^2 + a_2^2 + a_3^2 + 2a_1a_2\cos\theta_2 + 2a_1a_3\cos\theta_3 + 2a_2a_3\cos(\theta_2 - \theta_3)$.

V. Lowest MGF

In this section we demonstrate that, for both the NWDP and the FNR fading models, the MGF of the received signal power with a single specular component is always equal or lower than the MGF for arbitrary $N > 1$ for any given value of the variable. As we will later see, this will have implications on system performance analysis, as it entails that the error probability under Rician (or Rician shadowed) fading, i.e. when $N = 1$, is always lower than for any other N, for a given average signal-to-noise ratio (SNR).

Lemma 1: Let us consider either a NWDP or a FNR fading model and assume that the complex variable s in their MGF expressions takes a real value. Then, for a fixed total power of the specular as well as the diffuse components, the following inequality holds:

$$M_N(s) \geqslant M_1(s). \tag{37}$$

Proof: Let us first consider the NWDP fading model. Jensen's inequality states that given a random variable X, a real-valued function g and a convex function h, we can write

$$E_X\left[h\left(g(X)\right)\right] \geqslant h\left(E_X\left[g(X)\right]\right). \tag{38}$$

Let $h(x) = \exp(x)$ and $g(P_N) = P_N s/(1-\Omega_0 s)$. Thus, by virtue of Jensen's inequality, we can write

$$\begin{aligned} M_N(s) &= E_{P_N}\left[\frac{1}{1-\Omega_0 s}\exp\left(\frac{P_N s}{1-\Omega_0 s}\right)\right] \\ &\geqslant \frac{1}{1-\Omega_0 s}\exp\left(E_{P_N}\left[\left(\frac{P_N s}{1-\Omega_0 s}\right)\right]\right) \\ &= \frac{1}{1-\Omega_0 s}\exp\left(\frac{\Omega_N s}{1-\Omega_0 s}\right) \\ &= \frac{1}{1-\Omega_0 s}\exp\left(\frac{\Omega_1 s}{1-\Omega_0 s}\right) = M_1(s), \end{aligned} \tag{39}$$

where Ω_N was defined in (7) and represents the average power of the set of the N specular components, which is assumed to be the same for all N (i.e., $\Omega_1 = \Omega_2 = \ldots = \Omega_N$). Noting that the last equality in (39) is actually the exact expression of the MGF when $N = 1$ (Rician fading), denoted as $M_1(s)$, (37) is obtained.

Let us now consider the FNR fading model. It is worth noting that, conditioned on ζ, the FNR model defined in (22) is actually the NWDP model in (1) when parameters a_i in the NWDP model are substituted by $\sqrt{\zeta}a_i$. As (37) holds in this case for any particular realization of ζ, the inequality also holds after averaging over ζ, which yields the FNR MGF at both sides of the inequality. ■

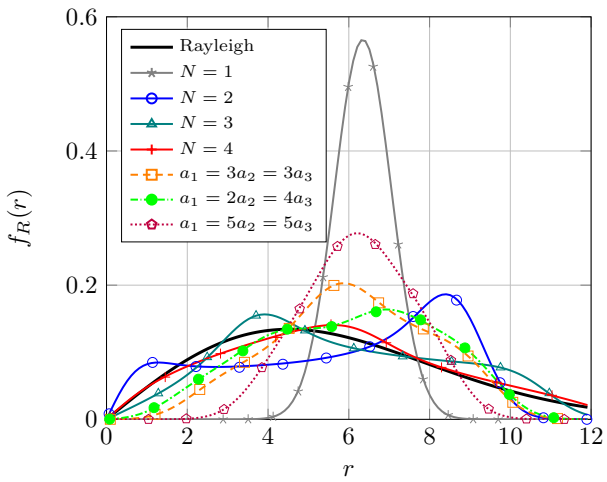

Fig. 1. Probability density function of the received signal amplitude under NWDP fading for different numbers of dominant specular waves N and different amplitude configurations. Parameter values are $K_{\text{dB}} = 16$ dB and $\Omega_0 = 1$. Solid lines correspond to the balanced amplitude cases. Markers denote MC simulations.

VI. Numerical evaluation

In this section, we present some illustrative results that exemplify the key characteristics of the NWDP and FNR models. Evaluation of the PDF and performance analysis are carried out, aiming to identify the impact of the different parameters of the models. We also include empirical verification for different scenarios, showing the ability of ray-based fading models to provide a better fit to channel measurements in different scenarios. Monte Carlo (MC) simulations have been included in the figures through markers in order to confirm the validity of the derived expressions. As in (10), we define a power ratio parameter similar to the conventional Rician K parameter as $K_N \triangleq \frac{\Omega_N}{\Omega_0}$, which will be useful in the sequel.

A. Effect of fading parameters

In order to better understand the effect of considering different numbers of specular components and their relative amplitudes, we evaluate the PDF of the NWDP and FNR models. Specifically, we represent the PDF of the received signal envelope R in Figs. 1 and 2, which are directly obtained from those of U using a simple transformation of random variables, i.e. $f_R(r) = 2r \cdot f_U(r^2)$.

Fig. 1 corresponds to the NWDP case, on which different parameter configurations have been chosen. We set $K_{\text{dB}} = 10\log_{10}(K_N) = 16$ dB[5] with $\Omega_0 = 1$, so that $E\{|R|^2\} = K_N + 1$, and two different situations: balanced amplitudes of the dominant waves ($a_i = a_j\,\forall i, j = 1 \ldots N$), as well as the unbalanced amplitude situation. The balanced

[5]A reasonably large value of K_{dB} is required in this setting since, as we back-off from the CLT assumption, the consideration of a larger number of individual waves implies a larger value of K_N, i.e., as N grows the amount of power associated to the diffuse components Ω_0 is reduced in the same amount as Ω_N is increased.

This article has been accepted for publication in IEEE Transactions on Vehicular Technology. This is the author's version which has not been fully edited and content may change prior to final publication. Citation information: DOI 10.1109/TVT.2022.3141949

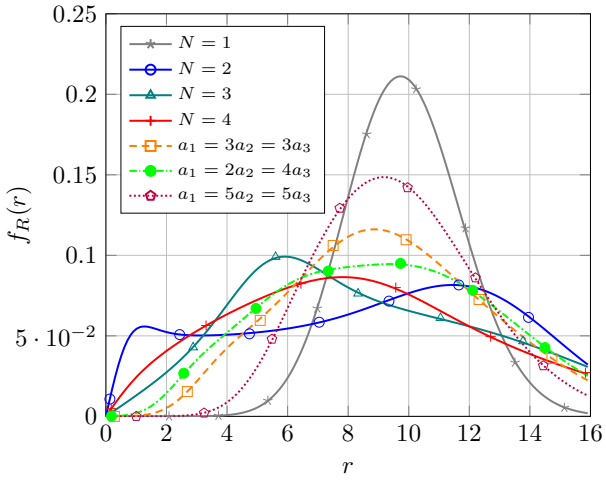

Fig. 2. Probability density function of the received signal amplitude under FNR fading for different numbers of dominant specular waves N and different amplitude configurations. Parameter values are $K_{\text{dB}} = 20$ dB, $\Omega_0 = 1$ and $m = 8$. Solid lines correspond to the balanced amplitude cases. Markers denote MC simulations.

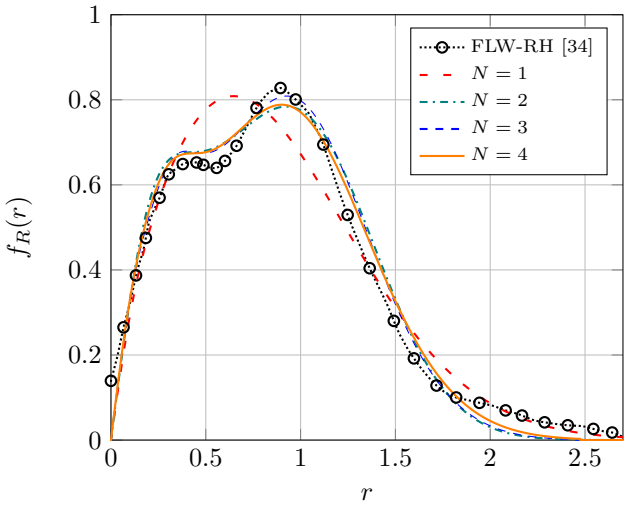

Fig. 3. Empirical PDF for the body-centric FLW-RH scenario presented in [34] vs. PDF fit using the FNR fading model, considering an increasing number of specular components. $\{N = 1,\ m = 0.85,\ a_1 = 0.99,\ \Omega_0 = 0.014,\ \text{rmse} = 0.072\}$; $\{N = 2,\ m = 4.7,\ a_1 = 0.70,\ a_2 = 0.56,\ \Omega_0 = 0.054,\ \text{rmse} = 0.049\}$; $\{N = 3,\ m = 5.2\, a_1 = 0.71,\ a_2 = 0.59,\ a_3 = 0.21, \Omega_0 = 0.01,\ \text{rmse} = 0.042\}$; $\{N = 4,\ m = 5,\ a_1 = a_2 = 0.65,\ a_3 = 0.19,\ a_4 = 0.18,\ \Omega_0 = 0.01,\ \text{rmse} = 0.041\}$

case is represented in the figure using solid lines, and the unbalanced case (with $N = 3$) is represented using discontinuous lines. The distribution density for Rayleigh fading is also shown in the figure for the sake of comparison. Let us first analyze the balanced scenario: we can see that the cases $N = 2$ and $N = 3$ correspond to very different PDF shapes compared to the Rician case ($N = 1$), and it leads to a non-unimodal behavior. In particular, for $N = 2$ the distribution becomes clearly bimodal and is concentrated mostly for high values of the variable r. It is worth mentioning the significant change of behavior for $N = 3$ and notably on the mode of the distribution, as in this case the distribution concentrates around lower values of r. For $N = 4$ we see that the shape of the PDF is rather different from the Rician case, and actually it starts to resemble that of a Rayleigh distribution. With regard to the unbalanced case, we see that modifying the relative amplitudes of the dominant waves has a direct impact on the shape of the PDF. As the unbalance of the power among specular components is more noticeable, the shape of the PDF tends to a Rician distribution (with a larger variance), because the power of the lower-amplitude components becomes similar to the diffuse component.

Fig. 2 illustrates the PDF of the received signal envelope under FNR fading using a similar set of parameters as those in Fig. 1. We now set a slightly larger $K_{\text{dB}} = 20$ dB and $m = 8$, which corresponds to a moderate fluctuation of the dominant components. We see that the effect of considering a random fluctuation on the dominant components somehow averages out the shape of the PDF compared to the deterministic case (i.e. NWDP). Increasing the number of waves or modifying their relative amplitudes has a similar effect as in the NWDP case.

B. Empirical validation

We now illustrate how these families of ray-based fading models are useful to recreate realistic fading conditions in different fading environments, which cannot be emulated by state-of-the-art fading models. First, we consider a body-centric scenario as in [34], on which a body sensor node placed in several positions communicates with receive antennas placed near the head, wrist and ankle. The carrier frequency used in the experiment is $f = 2.45$ GHz, and specific details for the measurement configuration are given in [34]. The empirical PDF for the front-left-waist to right-head measurements is represented in Fig. 3, together with the best fit provided by the FNR model using an increasing number of dominant specular waves. The Matlab curve fitting toolbox was used for this purpose, with the goal of minimizing the root mean square error (RMSE). We see that the FNR model with an increasing number of specular components is able to recreate the bimodal shape of the empirical PDF (measured in an anechoic chamber) in [34, Fig. 6] with increased accuracy when considering $N > 2$ dominant specular components. This is coherent with the nature of the FNR model: few dominant components (no major improvement is observed when moving from $N = 3$ to $N = 4$) with a virtually negligible diffuse component, and human-body shadowing captured through the parameter m. For $N = 4$, the improvement in terms of root mean square error (rmse) is insignificant compared to $N = 3$, as confirmed by the RMSE values provided by the Matlab curve fitting toolbox (see Fig. 3 caption for details).

The second set of empirical measurements used to validate our models is borrowed from [35], on which an outdoor mmWave link operating at 28 GHz was considered, and Rician fading was used for fitting purposes. Later results in [18] confirmed that the FTR fading model provided an improved fit; our goal here is to show that considering a larger number of dominant specular waves, i.e., a larger order FNR model, can improve the accuracy of the fitting to field measurements. In

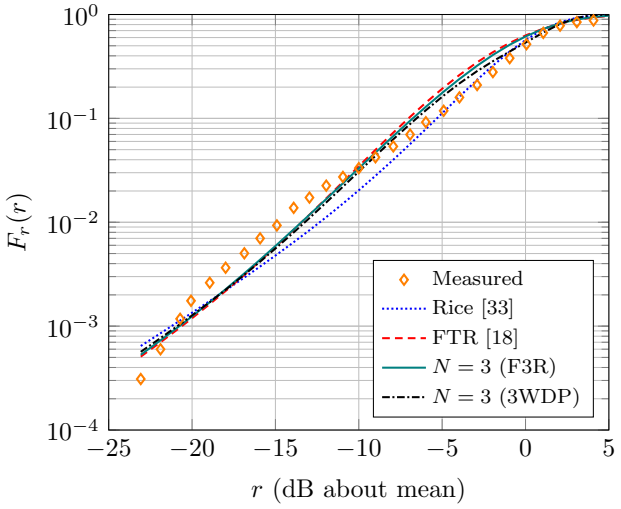

Fig. 4. Empirical vs theoretical CDFs of the received signal amplitude for LOS scenario [18, Fig. 8] and [35, Fig. 6, LOS]. Parameter values for Rician $\left[K^{\text{dB}}_{\text{Rice}} = 6.06\right]$, FTR $\left[K^{\text{dB}}_{\text{FTR}} = 19.03, a_1 = 0.95, a_2 = 0.31, m = 2\right]$, F3R $\left[K^{\text{dB}}_{\text{F3R}} = 20.35, a_1 = 0.98, a_2 = 0.147, a_3 = 0.098, m = 1.75\right]$ and 3WDP $\left[K^{\text{dB}}_{\text{3WDP}} = 14.05, a_1 = 0.864, a_2 = 0.432, a_3 = 0.173\right]$ are used. Error values are $\epsilon_{\text{Rice}} = 0.3302$, $\epsilon_{\text{FTR}} = 0.225$, $\epsilon_{\text{F3R}} = 0.207$ and $\epsilon_{\text{3WDP}} = 0.236$.

this case, similarly to [18], we aim to minimize an error factor ϵ that quantifies the goodness of fit between the empirical and theoretical CDFs of the received signal amplitude in log-scale, defined as:

$$\epsilon \triangleq \max_x \left| \log_{10} \hat{F}_r(x) - \log_{10} F_r(x) \right| \tag{40}$$

In Fig. 4, we present the results of the optimized fitting that minimizes ϵ for the cases of $N = 2 \ldots 4$ and FNR fading, and where the case of Rician fading given in [35] is also included as a reference. We observe that when $N = 3$, labeled as F3R for the sake of shorthand notation, the error parameter is reduced compared to the already good fit of the FTR case. The consideration of $N = 3$ for the NWDP case, labeled as 3WDP for the sake of shorthand notation, also provides a good fit to the measurement set, although slightly worse than with FTR. We see that the ability to model random fluctuations in the dominant specular components allows to model propagation in this scenario more accurately.

C. Average error rate

The bit/symbol error rate (BER/SER) performances over a large variety of modulations schemes can be computed using the MGF approach proposed by Simon and Alouini [25]. Hence, the results in (16)-(21) and (30)-(34) can be leveraged to analyze the error performances for different modulation schemes. In order to exemplify the implications of the lowest MGF results given in Section V, we will now focus on the error rate expression given by

$$\overline{P_e} = C_1 M_N(-b_1), \tag{41}$$

which is valid for differentially coherent detection, binary phase-shift-keying (DBPSK) or noncoherent detection of binary frequency-shift-keying (NCFSK), and where C_1 and b_1 are constants which depends on the modulation scheme, i.e., $b_1 = 1$ for DBPSK and $b_1 = 0.5$ for NCBFSK, with $C_1 = 0.5$ in both cases. Note that similar results can be obtained for the cases of coherent M-ary FSK or M-ary PSK [25], with

$$\overline{P_e} = C_2 \int_{\xi_1}^{\xi_2} h(\xi) M_N(-b_2 g(\xi)) d\xi, \tag{42}$$

where C_2 and b_2 are constants and g and h some given functions.

Inspection of (41) reveals that a direct application of the lowest MGF condition in Lemma 1 implies that, either for NWDP or FNR fading models, for any modulation scheme for which the average SER can be computed using (41) or (42), the minimum average error rate is obtained for $N = 1$ (i.e., Rician or Rician shadowed fading).

The average error rates assuming NCFSK modulation are plotted in Figs. 5 and 6, as a function of the average SNR $\overline{\gamma} = \frac{\Omega_N + \Omega_0}{N_0}$, with N_0 being the noise power. We consider an increasing number of rays $N = 1 \ldots 4$, as well as two situations for the relative amplitudes of the dominant specular waves: the balanced case with $a_i = a, \forall i = 1 \ldots N$, and the unbalanced case with $a_i = a/i, \forall i = 1 \ldots N$; these are labeled as (b) and (u), respectively, in the figures. The case of Rayleigh fading has been also included as a reference in both figures.

Either under NWDP fading (Fig. 5) or FNR fading (Fig. 6), the cases with $N = 1$ correspond to those with the lowest error rates. We see that the effect of having a balanced/unbalanced set of amplitudes for the dominant specular waves has an important effect specially in the case of $N = 2$, i.e., whenever the two dominant specular components are more likely to cancel each other. We also see that fluctuations on the specular components have a detrimental impact on performance. Notably, the case of Rayleigh fading is not always the worst case in terms of error rate, as in some instances the error performances under NWDP or FNR fading are associated to a worse-than-Rayleigh performance. This confirms that ray-based models are able to recreate hyper-Rayleigh conditions not only for $N = 2$ [36].

D. Outage probability

As a final application, we now evaluate the outage probability (OP) performance, in order to verify the accuracy of the asymptotic approximations for the CDFs derived throughout Sections III and IV. The instantaneous channel capacity per unit bandwidth is given by

$$C = \log_2(1 + \gamma), \tag{43}$$

where $\gamma = U/N_0$ is the instantaneous signal-to-noise ratio (SNR) and N_0 is the background noise. From this definition, the OP can be defined as the probability that the instantaneous channel capacity C falls below a predefined threshold R_S (given in terms of rate per unit bandwidth), i.e.,

$$P_{\text{out}} = P\left(C < R_S\right) = P\left(\log_2(1 + \gamma) < R_S\right), \tag{44}$$

or, equivalently,

$$P_{\text{out}} = P\left(\gamma < 2^{R_S} - 1\right) = F_\gamma\left(2^{R_S} - 1\right). \tag{45}$$

This article has been accepted for publication in IEEE Transactions on Vehicular Technology. This is the author's version which has not been fully edited and content may change prior to final publication. Citation information: DOI 10.1109/TVT.2022.3141949

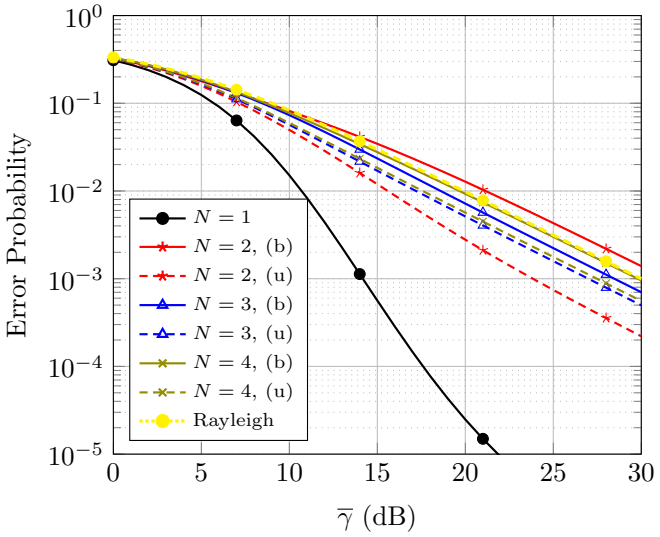

Fig. 5. Average error probability vs. average SNR for NWDP fading. Parameter values are $K_N = 10$, and $N = 1 \ldots 4$. Solid lines (b) correspond to balanced amplitudes, whereas dashed lines (u) correspond to unbalanced amplitudes. Rayleigh fading is included with dotted lines.

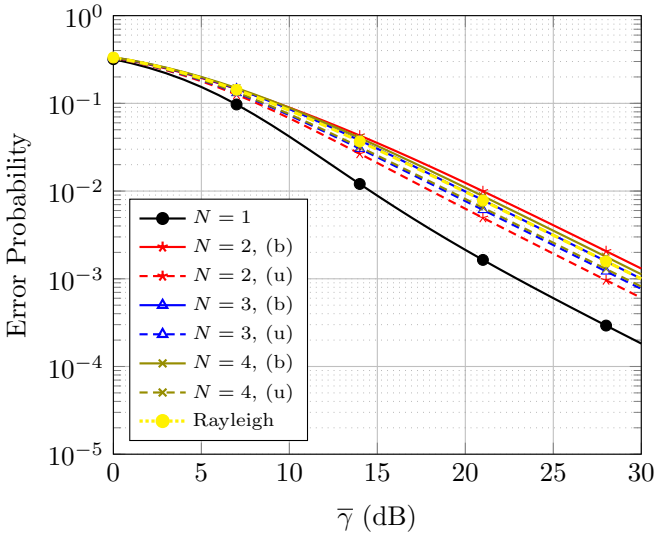

Fig. 6. Average error probability vs. average SNR for FNR fading. Parameter values are $K_N = 6$, $m = 4$ and $N = 1 \ldots 4$. Solid lines (b) correspond to balanced amplitudes, whereas dashed lines (u) correspond to unbalanced amplitudes. Rayleigh fading is included with dotted lines.

Thus, the OP can be directly calculated from (9) and (25) for the NWDP and FNR fading models, respectively, specialized for $\gamma = 2^{R_S} - 1$. As in Figs. 5 and 6, the average SNR is given by $\overline{\gamma} = E\{U\}/N_0$.

The OP is evaluated in Fig. 7, aiming to understand the impact of the number of dominant components in the system performance, as well as the range of validity of the asymptotic results. The balanced case is considered, and both the exact and the asymptotic outage probabilities are represented in the figure. A threshold rate $R_S = 1$ bps/Hz is set, and the fading parameter values are $K_{\text{dB}} = 14$ dB, and $m = 5$ for FNR fading. Similarly to the error rate performances, we see that the best performance is always attained for $N = 1$ (i.e. the Rician or Rician shadowed cases) for the operating range of OP values. As indicated in [19], the worst performance is achieved for the case $N = 2$; notably, the performance is even worse than in the Rayleigh case. Increasing the number of waves to $N = 3$ is beneficial for system performance compared to $N = 2$, and for $N = 4$ we see a very similar (although slightly worse) performance than in the Rayleigh case. In all instances, the performance under FNR fading is always worse than its NWDP counterpart. Finally, we note that the range of validity for the asymptotic expressions in (10) and (26) depends on the number of dominant specular components, and that a diversity order equal to one is observed.

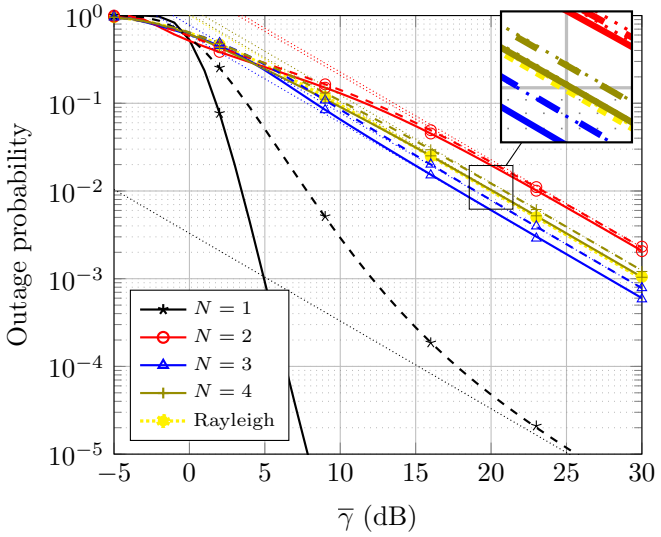

Fig. 7. Outage probability vs. average SNR, for different numbers of dominant specular waves N. The Rayleigh case is included as a reference (solid black line). Solid colored lines correspond to NWDP fading, and dashed lines correspond to the FNR case. Dotted thin lines are used for the asymptotic approximations using (9) and (26). Parameter values are $K_{\text{dB}} = 14$ dB, $m = 5$ and $R_S = 1$ bps/Hz. Markers denote MC simulations

VII. Conclusions

We have presented a comprehensive statistical characterization of the multipath wireless channel when an arbitrary number N of specular (dominant) waves (either with constant or random amplitudes) are received together with a diffuse component. The newly proposed class of fading models is able to modeling propagation conditions which largely differ from those captured by classical fading models like Rayleigh or Rician, but that also include these classical models as special cases.

The NWDP model is considered for the case when the specular wave components have constant amplitudes. It was shown that the statistical characterization and the performance metrics of this model can be derived from the Rician fading model, and performing $N - 1$ easy-to-compute finite range integrations over the phases of the received specular components. Alternatively, the NWDP model can be also derived from the TWDP model and performing only $N - 2$ integrations. On the other hand, the FNR model is proposed for the case when the amplitudes of the specular component

experience random fluctuations. In this case the model can be derived from either the Rician shadowed or the FTR fading models by performing, respectively, $N-1$, or $N-2$ integrations.

We have shown that the best performance results are obtained when there is only one specular component. Mathematically, increasing the number of specular components gives additional degrees of freedom, and could allow to ideally account for even arbitrarily small specular components. However, in practice the improvement obtained when considering a larger number of specular components is limited by the actual resolution of the channel sounding process, which provides imperfect channel estimates. Hence, the additional benefits of considering more that 4 specular components is often negligible, therefore, in practice, only a single or double simple finite-range integration is required for the relevant cases of, respectively, $N=3$ and $N=4$ specular components.

The work presented here, rather than being a simple extension of the well known fading models for $N=1$ and $N=2$, shows that dramatic changes can be expected in the received power (or envelope) distribution when $N=3$ with respect to the $N=2$ case, notably on the mode of the distribution density. Actually, a major benefit of the presented models with respect to other state-of-the-art fading models relays on the versatility and the very different shapes of the distribution density that can be obtained by varying the models parameters, permitting to concentrate the power distribution values and its main mode at either low or high values of the received power, which is unattainable for the models with $N \leq 2$. Thus, the presented models can be used to analyze the performance of a wider range of wireless fading scenarios. For instance, the impact of considering an increasing number of specular components on the beamforming design can be quantified [37]. Similarly, coordinated beamforming schemes aimed at reducing interference [38] can also be considered. As pointed out in [38], the zero-forcing solution becomes more complicated as more specular components are considered, so the development of low-cost zero-forcing solutions seems an interesting line for future research activities.

REFERENCES

[1] A. Osseiran et al., "Scenarios for 5G mobile and wireless communications: the vision of the METIS project," *IEEE Commun. Mag.*, vol. 52, no. 5, pp. 26–35, May 2014.

[2] K. Haneda et al., "5G 3GPP-like channel models for outdoor urban microcellular and macrocellular environments," in *IEEE 83rd Vehicular Technology Conference (VTC Spring)*, May 2016, pp. 1–7.

[3] S. Hur, S. Baek, B. Kim, Y. Chang, A. F. Molisch, T. S. Rappaport, K. Haneda, and J. Park, "Proposal on millimeter-wave channel modeling for 5G cellular system," *IEEE J. Sel. Topics Signal Process.*, vol. 10, no. 3, pp. 454–469, April 2016.

[4] P. Beckmann, "Statistical distribution of the amplitude and phase of a multiply scattered field," *J. Res. Natl. Bur. Stand. D. (U.S.)*, vol. 66D, no. 3, pp. 231–240, 1962.

[5] Y. Niu, Y. Li, D. Jin, L. Su, and A. V. Vasilakos, "A survey of millimeter wave communications (mmWave) for 5G: opportunities and challenges," *Wireless Networks*, vol. 21, no. 8, pp. 2657–2676, Nov 2015.

[6] P. C. F. Eggers, M. Angjelichinoski, and P. Popovski, "Wireless channel modeling perspectives for ultra-reliable communications," *IEEE Trans. Wireless Commun.*, vol. 18, no. 4, pp. 2229–2243, 2019.

[7] P. Ramírez-Espinosa, R. J. Sánchez-Alarcón, and F. J. López-Martínez, "On the beneficial role of a finite number of scatterers for wireless physical layer security," *IEEE Access*, vol. 8, pp. 105 055–105 064, 2020.

[8] L. Subrt and P. Pechac, "Intelligent walls as autonomous parts of smart indoor environments," *IET Commun.*, vol. 6, no. 8, pp. 1004–1010, May 2012.

[9] Q. Wu and R. Zhang, "Intelligent reflecting surface enhanced wireless network: joint active and passive beamforming design," in *IEEE Global Commun. Conf. (GLOBECOM)*, Dec 2018, pp. 1–6.

[10] M. Slack, "The probability distributions of sinusoidal oscillations combined in random phase," *J. Inst. Electr. Eng. 3*, vol. 93, no. 22, pp. 76–86, March 1946.

[11] S. Rice, "Probability distributions for noise plus several sine waves - the problem of computation," *IEEE Trans. Commun.*, vol. 22, no. 6, pp. 851–853, June 1974.

[12] M. Simon, "On the probability density function of the squared envelope of a sum of random phase vectors," *IEEE Trans. Commun.*, vol. 33, no. 9, pp. 993–996, Sep. 1985.

[13] C. W. Helstrom, "Distribution of the envelope of a sum of random sine waves and Gaussian noise," *IEEE Trans. Aerosp. Electron. Syst.*, vol. 35, no. 2, pp. 594–601, April 1999.

[14] G. D. Durgin, "Theory of stochastic local area channel modeling for wireless communications," Ph.D. dissertation, Virginia Tech, 2000.

[15] A. Abdi, H. Hashemi, and S. Nader-Esfahani, "On the PDF of the sum of random vectors," *IEEE Trans. Commun.*, vol. 48, no. 1, pp. 7–12, Jan 2000.

[16] G. D. Durgin, T. S. Rappaport, and D. A. de Wolf, "New analytical models and probability density functions for fading in wireless communications," *IEEE Trans. Commun.*, vol. 50, no. 6, pp. 1005–1015, June 2002.

[17] M. Rao, F. J. Lopez-Martinez, M.-S. Alouini, and A. Goldsmith, "MGF approach to the analysis of generalized two-ray fading models," *IEEE Trans. Wireless Commun.*, vol. 14, no. 5, pp. 2548–2561, May 2015.

[18] J. M. Romero-Jerez, F. J. Lopez-Martinez, J. F. Paris, and A. J. Goldsmith, "The fluctuating two-ray fading model: Statistical characterization and performance analysis," *IEEE Trans. Wireless Commun.*, vol. 16, no. 7, pp. 4420–4432, July 2017.

[19] C. C. Chai and T. T. Tjhung, "Unified Laguerre polynomial-series-based distribution of small-scale fading envelopes," *IEEE Trans. Veh. Technol.*, vol. 58, no. 8, pp. 3988–3999, Oct 2009.

[20] Y. J. Chun, "A generalized fading model with multiple specular components," *arXiv preprint arXiv:1810.05258*, 2018.

[21] J. B. Andersen, "Statistical distributions in mobile communications using multiple scattering," in *Proc. 27th URSI General Assembly*, 2002, pp. 1–4.

[22] J. Salo, H. M. El-Sallabi, and P. Vainikainen, "Statistical Analysis of the Multiple Scattering Radio Channel," *IEEE Trans. Antennas Propag.*, vol. 54, no. 11, pp. 3114–3124, Nov 2006.

[23] F. J. Scire, "A probability density function theorem for the modulo y values of the sum of two statistically independent processes," *Proc. IEEE*, vol. 56, no. 2, pp. 204–205, Feb 1968.

[24] Z. Wang and G. Giannakis, "A Simple and General Parameterization Quantifying Performance in Fading Channels," *IEEE Trans. Commun.*, vol. 51, no. 8, pp. 1389–1398, Aug. 2003.

[25] M. K. Simon and M.-S. Alouini, *Digital communication over fading channels*. Wiley-IEEE Press, 2005.

[26] C. Chen and A. Abdi, "Bit error rate in multipath wireless channels with several specular paths," *Electron. Lett.*, vol. 47, no. 18, pp. 1046–1048, Sep. 2011.

[27] J. P. Peña-Martín, J. M. Romero-Jerez, and F. J. Lopez-Martinez, "Generalized MGF of the two-wave with diffuse power fading model with applications," *IEEE Trans. Veh. Technol.*, vol. 67, no. 6, pp. 5525–5529, 2018.

[28] A. Abdi, W. Lau, M.-S. Alouini, and M. Kaveh, "A new simple model for land mobile satellite channels: first- and second-order statistics," *IEEE Trans. Wireless Commun.*, vol. 2, no. 3, pp. 519–528, May 2003.

[29] J. F. Paris, "Closed-form expressions for Rician shadowed cumulative distribution function," *Electron. Lett.*, vol. 46, no. 13, pp. 952–953, June 2010.

[30] P. W. K. H. M. Srivastava, *Multiple Gaussian Hypergeometric Series*. John Wiley & Sons, 1985.

[31] J. F. Paris, "Statistical characterization of κ-μ shadowed fading," *IEEE Trans. Veh. Technol.*, vol. 63, no. 2, pp. 518–526, Feb 2014.

[32] I. S. Gradshteyn and I. M. Ryzhik, *Table of integrals, series and products*, 7th ed. Academic Press Inc, 2007.

[33] M. Abramowitz and I. A. Stegun, *Handbook of mathematical functions with formulas, graphs, and mathematical tables*. 10th ed. U.S. Department of Commerce - N.B.S., Dec. 1972.

[34] S. L. Cotton, "A statistical model for shadowed body-centric communications channels: theory and validation," *IEEE Trans. Ant. Prop.*, vol. 62, no. 3, pp. 1416–1424, Mar. 2014.
[35] M. K. Samimi, G. R. MacCartney, S. Sun, and T. S. Rappaport, "28 GHz millimeter-wave ultrawideband small-scale fading models in wireless channels," in *2016 IEEE 83rd Vehicular Technology Conference (VTC Spring)*, May 2016.
[36] C. Garcia-Corrales, U. Fernandez-Plazaola, F. J. Cañete, J. F. Paris, and F. J. Lopez-Martinez, "Unveiling the hyper-Rayleigh regime of the fluctuating two-ray fading model," *IEEE Access*, vol. 7, pp. 75 367–75 377, 2019.
[37] S. Schwarz, "Outage Investigation of Beamforming Over Random-Phase Finite-Scatterer MISO Channels," *IEEE Signal Process. Lett.*, vol. 24, no. 7, pp. 1029–1033, 2017.
[38] S. Schwarz and M. Rupp, "Reliable Multi-Point Transmissions Over Directional MISO TWDP Fading Channels," *IEEE Trans. Veh. Technol.*, vol. 70, no. 2, pp. 1394–1409, 2021.

Juan M. Romero-Jerez (Senior Member, IEEE) received the M.Sc. degrees both in telecommunications engineering and mathematics from the University of Malaga, Spain, and the Ph.D. degree in telecommunications engineering from the University of Malaga, in 2001. In 1996, he joined the Electronic Technology Department, University of Malaga, where he is currently a Full Professor. He was a Visiting Associate Professor with the Electrical Engineering Department, Stanford University, from September 2005 to February 2006, from September 2007 to February 2008, and also from February 2016 to March 2016. He has participated in several research projects in the areas of packet radio transmission, multiple antennas, interference management, and cellular networks. His current research interest is in the area of wireless communications and, more specifically: wireless communications performance analysis, multipath fading, wireless channel modeling, diversity systems, smart antennas, MIMO performance, and interference management. He was an Editor of the IEEE TRANSACTIONS ON WIRELESS COMMUNICATIONS between 2015-2020.

F. Javier López-Martínez (Senior Member, IEEE) received the M.Sc. and Ph.D. degrees in Telecommunication Engineering from the University of Málaga (Spain), in 2005 and 2010, respectively. He was a Marie Curie postdoctoral fellow in the Wireless Systems Lab at Stanford University (2012-2014), and at University of Málaga (2014-2015). Since 2015, he has been a faculty member with the Communication Engineering Department, University of Málaga, where he is now an Associate Professor. He has been a Visiting Researcher with University College London, in 2010, and Queen's University Belfast, in 2018.

His research interests include a diverse set of topics in the wide areas of communication theory and wireless communications, including stochastic processes, wireless channel modeling, physical layer security, and wireless powered communications. He has received several research awards, including the Best Paper Award from the Communication Theory Symposium at the IEEE GLOBECOM 2013, the IEEE Communications Letters Exemplary Reviewer Certificate in 2014 and 2019, and the IEEE Transactions on Communications Exemplary Reviewer Certificate, in 2014, 2016 and 2019. He is an Editor of the IEEE Transactions on Communications, in the area of wireless communications, and a Senior Member of the IEEE.

Juan P. Peña-Martin (Senior Member, IEEE) received the M.Sc. degree in physics from the University of Granada, Spain, in 1986, and the Ph.D. degree from the University of Málaga, Spain, in 2009. He is currently an Associate Professor with the Electronic Technology Department, University of Málaga, Spain. He started his cooperation with the University of Málaga in 1988, as a part-time Lecturer. From 1986 to 1992, he was a Hardware Engineer with the Research and Development Department, Fujitsu España, SA, and, for one year, with the Kawasaki Laboratories, Fujitsu Limited. From 1992 to 2003, he was with AT4-Wireless, where he held various positions. From 2003 to 2007, he was a Freelance Consultant for testing laboratories. His research interests are in the areas of wireless communications performance analysis, multipath fading, wireless channel modeling, diversity systems, and MIMO performances.

Ali Abdi (Fellow, IEEE) received the Ph.D. degree in electrical engineering from the University of Minnesota, Minneapolis. He joined the Department of Electrical and Computer Engineering of New Jersey Institute of Technology (NJIT), Newark, where he is currently a Professor. His research interests include wireless communication in underwater, terrestrial and pipeline channels, characterization and estimation of communication channels, vector acoustic communication and signal processing, blind modulation recognition, molecular networks and systems biology. He is a Fellow of IEEE.